ARTICLE

OPEN

Check for updates

Mineral evolution facilitated Earth's oxidation

Haitao Shang [1 ✉]

Oxygenation events remarkably altered the distribution, diversity, and abundance of minerals on Earth's surface. However, the causality in the opposite direction—the influence of mineral evolution on atmospheric oxygen levels—has rarely been explored. Here I propose that mineral evolution might have led Earth's oxygen cycle to lose stability, facilitating oxygenation events in deep time. First, I introduce a conceptual model for the system of organic matter and minerals and investigate their interactions via a probabilistic approach. Second, in light of the theoretical results, I suggest that the evolution of iron and clay minerals likely had an underappreciated relevance to the Great Oxidation Event and Neoproterozoic Oxidation Event, respectively. Finally, I use the parameter values estimated from observations in modern environments as benchmarks to test these speculations. This study provides a minimalistic theoretical framework illustrating the possible influence of mineral evolution on Earth's oxygen cycle over geologic time.

---

[1] Institute of Ecology and Evolution, University of Oregon, Eugene 97403 OR, USA. ✉email: htshang.research@gmail.com

Molecular oxygen (O_2) is an important feature of the modern Earth's atmosphere. However, why and how Earth evolved from the ancient O_2-deficient environment to the modern O_2-rich world remain mysterious. Geological and geochemical studies have revealed two rapid and irreversible transitions of Earth's atmospheric oxygen levels (pO_2) that occurred ~2.4–2.3 billion years ago (Ga) and 0.8–0.54 Ga, which are also known as the Great Oxidation Event (GOE) and Neoproterozoic Oxidation Event (NOE), respectively[1,2]. Oxygenation events remarkably altered geochemical characteristics such as the distribution, diversity, and abundance of minerals on Earth's surface[3,4]. The information stored in sedimentary minerals therefore provides a window through which to investigate the evolution of the redox state of ancient Earth's surface environment[5,6]. However, the causality in the reverse direction—whether and how mineral evolution contributed to the oxygenation events—remains understudied[7].

Oxygen, a product of the three-billion-year-old biological invention of oxygenic photosynthesis, is consumed by aerobic respiration or oxidation of reducing compounds[1,2]. The existence of the redox couple of organic matter and O_2, more generally known as the carbon cycle, implies that the supply of O_2 in the environment is quantitatively related to detrital organic matter. A tiny leakage in the carbon cycle has been widely considered one major mechanism responsible for the accumulation of O_2 in Earth's atmosphere-ocean system: a small portion of organic matter produced by oxygenic photosynthesis is buried in sediments and loses the opportunity to react with O_2, resulting in the rise of O_2 levels[8,9].

The long-term persistence of organic matter in natural environments is a consequence of its intrinsic recalcitrance, extrinsic environmental factors, or both[10,11]. Intrinsically recalcitrant organic matter is resistant to degradation due to its stable structures and strong chemical bonds[12,13]. For example, humified organic matter formed in soils and sediments consists of an intricate series of aliphatic/aromatic compounds and is persistent at the geologic timescale[14,15]. The other instance is graphitized petrogenic carbon, which is extremely resilient with repeated exposure to oxygenated environments and can survive multiple episodes of recycling[12,13,16]. Physical, chemical, and biological variables in surrounding environments significantly influence organic preservation as well[10,11]. For example, in the water column of lakes and oceans, microbial consumption can transform an organic matter system to a new ensemble in which the low concentrations of individual components prevent further uptake by microorganisms; this mechanism is also referred to as the "dilution hypothesis"[17,18]. Organic matter can also be associated with minerals in soils and sediments via ligand exchange, cation bridging, Van der Waals force, and hydrogen bonding[19,20], which protects organic matter from the attacks of microorganisms and their digestive agents (e.g., carbon-degrading enzymes)[11,20]. This mechanism, also called "physical protection", makes extensive contributions to the long-term preservation of organic matter[11,21]. Although these mechanisms responsible for the persistence of organic matter are observed in the modern environment, they are expected to have been the same or similar on the ancient Earth[13,22].

In this study, I focus on the effects of physical protection on O_2 accumulation and explore how the microscopic interactions between organic matter and minerals might have influenced the macroscopic evolution of Earth's oxygen cycle in deep time. I first introduce a conceptual model to describe the system of organic matter and minerals and investigate the probabilistic properties of their interactions. I then show theoretically that adsorption/desorption of organic matter onto/off mineral surfaces are asymmetric and the former plays a dominant role. Analyses of the model predict that, under O_2-limiting conditions, the negative feedback stabilizing the modern Earth's oxygen cycle is unlikely to operate before the O_2 level exceeds a threshold and mineral surface capacity is saturated. Based on these results, I speculate that mineral evolution in the ancient O_2-deficient environment might have increased the capacity for organic matter adsorption and led Earth's oxygen cycle to lose stability, facilitating the accumulation of O_2. Finally, to test this speculation, I explore the possible contributions of iron(III) and clay minerals to the GOE and NOE, respectively, with the parameter values estimated from modern field observations as benchmarks. The results presented in this work provide a further step toward understanding the role of minerals in Earth's oxidation.

Results and discussion

A conceptual model for organic matter-mineral systems. To investigate the effects of organic matter-mineral interactions on organic burial and O_2 accumulation, I first consider the degradation of unprotected (y_1) and protected (y_2) organic matter in an aerobic environment. Figure 1 shows a conceptual model for the
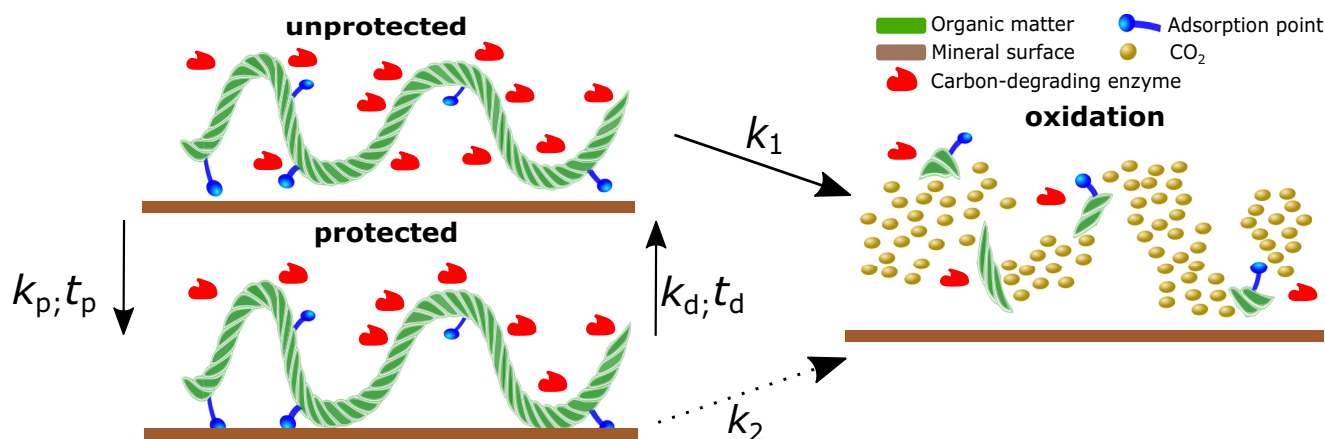

Fig. 1 Degradation paths of organic matter that is protected or unprotected by minerals. Unprotected organic matter is either directly oxidized to CO_2 with constant k_1 or adsorbed onto a mineral surface with rate constant k_p. The physically protected organic matter needs to be dissociated from the mineral surface (with rate constant k_d) before it can be degraded. The protected portion decays to CO_2 with rate constant k_2. The dashed arrow for k_2 indicates that the transformation of protected organic matter to CO_2 includes two steps: (1) dissociation from mineral surfaces with k_d and (2) oxidation to CO_2 with k_1. The characteristic times of adsorption and desorption are denoted by t_p and t_d, respectively.

interactions of organic matter with mineral surfaces and its degradation paths. The y_1 component is either directly oxidized to CO_2 with rate constant k_1 or transformed to the y_2 component (i.e., associated with minerals) with rate constant k_p, and the y_2 component is oxidized to CO_2 with rate constant k_2. The degradation of the y_2 component consists of two subprocesses (Fig. 1): (1) dissociation from mineral surfaces with rate constant k_d and (2) oxidation to CO_2 with rate constant k_1. Since this study focuses on the influence of mineral protection on the degradation/preservation of organic matter, I assume that organic matter desorbed from mineral surfaces is rapidly oxidized to CO_2 and the degradation rate of the y_2 component is dominated by its desorption rate: $k_2 \simeq k_d$.

Conventionally, the degradation of organic matter and its adsorption/desorption on mineral surfaces are expressed in terms of the first-order kinetics[23–26]. Here, I write the rates of changes in the protected and unprotected components at time t as

$$\frac{dy_1}{dt} = -k_1 y_1 - k_p y_1 + k_d y_2 \qquad (1)$$

$$\frac{dy_2}{dt} = k_p y_1 - k_d y_2. \qquad (2)$$

I denote the total amount of organic carbon and the fraction of the y_2 component at time $t = 0$ by $y_0 = y_1(0) + y_2(0)$ and f, respectively. The initial conditions then read $y_1(0) = y_0(1 - f)$ and $y_2(0) = y_0 f$. For the sake of simplicity, I introduce dimensionless rate constants $\kappa_p = k_p/k_1$, $\kappa_2 = k_2/k_1$ and $\kappa_d = k_d/k_1$, and dimensionless time $\tau = k_1 t$.

Under oxic conditions, degradation time t in Eqs. (1)–(2) is conventionally referred to as the oxygen-exposure time, which is the length of time during which organic matter is exposed to O_2[10,27]. I denote oxygen-exposure time and its dimensionless form as t_{O_2} and τ_{O_2}, respectively. Oxygen-exposure time is positively correlated with the atmospheric O_2 levels[10,27]: $\tau_{O_2} \propto pO_2$. The amount of physically protected organic matter after being exposed to O_2 for τ_{O_2} is then denoted as $y_2(\tau_{O_2})$. In the absence of O_2, some types of organic compounds, especially unprotected components, can be degraded by microorganisms with weaker electron acceptors (e.g., nitrate and sulfate)[10,28,29]. However, the degradation of the protected portion, which requires more energy to overcome the activation barriers, becomes slow or even ceases when O_2 is completely consumed or when organic matter is transported/sequestered into O_2-free environments, where the energetic rewards of organic degradation to microorganisms are poor[10,11,30]. Here, I identify $y_2(\tau_{O_2})$ as the amount of organic matter protected by minerals in marine sediments, where most of the organic matter burial on Earth takes place[11,13,27]; this is also the portion contributing to O_2 accumulation in the system of Eqs. (1)–(2). The initial fraction of the y_2 component (i.e., $f = y_2(0)/y_0$) thus also represents the burial efficiency when $\tau_{O_2} = 0$. Table 1 summarizes the variables and parameters in this study.

Probabilistic properties of organic matter-mineral interactions. To investigate organic matter-mineral interactions in natural environments, I consider an ensemble consisting of biopolymers with different compositions, lengths, and structures; these polymers are stochastically adsorbed onto or desorbed off mineral surfaces. Theoretical models[31,32] and experimental observations[33,34] have suggested that the (dimensionless) characteristic times for a polymer to be adsorbed onto and desorbed off a mineral surface can be expressed as $\tau_p \propto \exp(-M\psi)$ and $\tau_d \propto \exp(M\psi)$, respectively, where M is the molecular mass of the polymer and ψ is a parameter depending on other variables influencing the polymer-mineral interaction. Here, instead of following such a convention

expressing molecular mass as a separate factor, I rewrite the two characteristic times as $\tau_p \propto \exp(-\alpha)$ and $\tau_d \propto \exp(\alpha)$, in which α is an overall factor characterizing the polymer-mineral interaction.

The interactions between biopolymers and mineral surfaces are affected by a variety of physical, chemical, and biological variables, such as temperature, pH, the mass and functional group(s) of a biopolymer, the area and charge capacity of a mineral surface, and microbial enzymes[11,20,25]. I denote individual factors corresponding to each of these variables by $\beta_{i \in [0, N]}$ and assume that β_i's are independent and identically distributed (i.i.d.). This assumption of i.i.d. is an idealization because some factors influencing the adsorption/desorption of biopolymers onto/off mineral surfaces may depend on each other and their distributions may vary across different types of biopolymers and minerals. The overall factor α is then rewritten as $\alpha = \sum_{i=0}^{N} \beta_i$, where each β_i characterizes the influence of one variable on adsorption/desorption times. Since $\kappa_p = 1/\tau_p$ and $\kappa_d = 1/\tau_d$, I substitute this expression of α into the exponential relation between $\tau_{j \in \{p, d\}}$ and α introduced above and express these two rate constants by

$$\kappa_p \propto \exp\left(\sum_{i=0}^{N} \beta_i\right) \quad \text{and} \quad \kappa_d \propto \exp\left(-\sum_{i=0}^{N} \beta_i\right). \qquad (3)$$

Organic matter is highly heterogeneous; so, too, is the environment in which it interacts with minerals[11,20,24,35]. To obtain the average κ_p and κ_d for an organic matter-mineral system, I first calculate the probability distribution of κ_p and κ_d. To do so, I take the logarithm of both sides of Eq. (3) and obtain $\log(\kappa_p) \propto \sum_{i=0}^{N} \beta_i$ and $\log(\kappa_d) \propto -\sum_{i=0}^{N} \beta_i$. For a sufficiently large N, the Central Limit Theorem implies that the variable $\log(\kappa_j)$ satisfies

$$P\left(\log(\kappa_j)\right) \rightarrow \exp\left[-\frac{(\log(\kappa_j) - \mu_j)^2}{2\sigma_j^2}\right], \quad j \in \{p, d\} \qquad (4)$$

in which μ_j and σ_j^2 represent the mean and variance, respectively, of the probability distribution. Mathematically, $\mu_p \propto \sum_{i=0}^{N} \langle \beta_i \rangle$, $\mu_d \propto -\sum_{i=0}^{N} \langle \beta_i \rangle$, and $\sigma_p^2 = \sigma_d^2 \propto \sum_{i=0}^{N} \text{Var}(\beta_i)$, where $\langle \cdot \rangle$ and $\text{Var}(\cdot)$ represent the expectation and variance of a quantity, respectively. To calculate the probability distribution of κ_j, I change $P(\log(\kappa_p))$ to $P(\kappa_p)$ via the Jacobian transformation: $P(\kappa_j) = \frac{d \log(\kappa_j)}{d\kappa_j} P(\log(\kappa_j)) \sim (1/\kappa_j) \exp\left[-2\left(\frac{\log(\kappa_j) - \mu_j}{2\sigma_j}\right)^2\right]$. Away from the two tails of the distribution (i.e., $|\log(\kappa_j) - \mu_j| \ll 2\sigma_j$), the value of the exponential function approximates 1 and therefore the probability distribution of κ_j is

$$P(\kappa_j) \sim \frac{1}{\kappa_j}, \quad j \in \{p, d\}. \qquad (5)$$

The $P(X) \sim 1/X$ distribution in Eq. (5) appears in many physical and biological systems[36,37]. However, to my knowledge, this study suggests for the first time that this distribution likely exists in organic matter-mineral interactions (i.e., adsorption and desorption) as well. Moreover, the $P(X) \sim 1/X$ distribution is a common property of relaxation processes such as the aging of molecular and electron glasses[38,39], variation of protein states[40,41], and evolution of frictional strength[42,43]. These processes generally exhibit logarithmic-time decay (i.e., relaxation processes decay with the logarithm of time)[36,37]. The relaxation (e.g., conformational changes and reorientations) of biopolymers occurring in organic matter-mineral interactions[11,20] and the logarithmic-time degradation of organic matter in natural ecosystems[11,35] both support the $P(\kappa_j) \sim 1/\kappa_j$ distribution predicted in this study.

Table 1 Symbols, physical meanings, dimensionless forms, and mathematical relations of variables.

Symbol	Physical meaning	Dimensionless form	Mathematical relation
y_1	Organic matter unprotected by minerals	–	–
y_2	Organic matter protected by minerals	–	–
k_1	Rate constant for the oxidation of y_1 to CO_2	κ_1	–
k_2	Rate constant for the oxidation of y_2 to CO_2	κ_2	–
k_p	Adsorption rate constant	κ_p	–
k_d	Desorption rate constant	κ_d	–
t_p	Characteristic time of adsorption	τ_p	–
t_d	Characteristic time of desorption	τ_d	–
t	Time	τ	–
t_{O_2}	Oxygen-exposure time	τ_{O_2}	–
y_0	Initial total amount of y_1 and y_2	–	–
f	Initial fraction of y_2 over y_0	–	$f = y_2(0)/y_0$
α	Overall factor characterizing mineral-organic matter interactions	–	$\alpha = \sum_{i=0}^{N} \beta_i$
$\beta_{i\in[0,N]}$	Factors characterizing individual variables influencing mineral-organic matter interactions	–	–
$\mu_{j\in\{p,d\}}$	Mean in the probability distribution of $\log(\kappa_j)$, where $j \in \{p,d\}$	–	$\mu_p \propto \sum_{i=0}^{N} \langle \beta_i \rangle$ and $\mu_d \propto -\sum_{i=0}^{N} \langle \beta_i \rangle$
$\sigma^2_{j\in\{p,d\}}$	Variance in the probability distribution of $\log(\kappa_j)$, where $j \in \{p,d\}$	–	$\sigma^2_p = \sigma^2_d \propto \sum_{i=0}^{N} \mathrm{Var}(\beta_i)$
$k_{p,max}$	Maximum adsorption rate constant	$\kappa_{p,max}$	$k_{p,max} \simeq \langle k_p \rangle / \langle k_d \rangle$
$k_p^\star$	Critical value of $k_{p,max}$	$\kappa_p^\star$	$\kappa_p^\star = f/(1-f)$
R	Measurement of the change in $k_{p,max}$ required to destabilize the oxygen cycle	–	$R = \kappa_p^\star / \kappa_{p,max}$

With the probability distribution of κ_j (Eq. (5)), I calculate its average, $\langle \kappa_j \rangle$, over $[\kappa_{j,min}, \kappa_{j,max}]$. I first normalize the probability distribution of κ_j and obtain its density function: $p(\kappa_j) = (1/\kappa_j)/[\int_{\kappa_{j,min}}^{\kappa_{j,max}}(1/\kappa_j)d\kappa_j] = (1/\kappa_j)/\log(\kappa_{j,max}/\kappa_{j,min})$. The denominator, $\log(\kappa_{j,max}/\kappa_{j,min})$, is a normalization factor that guarantees the summation of $p(\kappa_j)$ between $\kappa_{j,min}$ and $\kappa_{j,max}$ to be 1. The expectation of κ_j, i.e., $\langle \kappa_j \rangle = \int_{\kappa_{j,min}}^{\kappa_{j,max}} \kappa_j p(\kappa_j) d\kappa_j$, then is

$$\langle \kappa_j \rangle = \frac{\kappa_{j,max} - \kappa_{j,min}}{\log(\kappa_{j,max}/\kappa_{j,min})}, \quad j \in \{p,d\}. \tag{6}$$

Dominance of adsorption processes. To explore the relation between $\langle \kappa_p \rangle$ and $\langle \kappa_d \rangle$, both of which depend on the overall factor α, I denote the range of α as $[\alpha_{min}, \alpha_{max}]$. Correspondingly, the lower and upper limits of κ_p are $\kappa_{p,min} \simeq \exp(\alpha_{min})$ and $\kappa_{p,max} \simeq \exp(\alpha_{max})$, respectively; the lower and upper limits of κ_d are $\kappa_{d,min} \simeq \exp(-\alpha_{max})$ and $\kappa_{d,max} \simeq \exp(-\alpha_{min})$, respectively. I substitute $\kappa_{p,min}, \kappa_{p,max}, \kappa_{d,min}$, and $\kappa_{d,max}$ into Eq. (6) and obtain $\langle \kappa_p \rangle \simeq [\exp(\alpha_{max}) - \exp(\alpha_{min})]/(\alpha_{max} - \alpha_{min})$ and $\langle \kappa_d \rangle \simeq [\exp(-\alpha_{min}) - \exp(-\alpha_{max})]/(\alpha_{max} - \alpha_{min})$. The ratio between these two average rate constants is $\langle \kappa_p \rangle / \langle \kappa_d \rangle \simeq [\exp(\alpha_{max}) - \exp(\alpha_{min})]/[\exp(-\alpha_{min}) - \exp(-\alpha_{max})]$. Since organic matter-mineral systems and the physical, chemical, and biological conditions of their surrounding environments are highly heterogeneous[11,20,24], I assume that the overall factor α, which characterizes the influence of these factors on organic matter-mineral interactions, has a wide range: $\alpha_{min} \ll \alpha_{max}$, implying that $\exp(\alpha_{min}) \ll \exp(\alpha_{max})$ and $\exp(-\alpha_{max}) \ll \exp(-\alpha_{min})$. With these two inequalities, I rewrite the above expression of the ratio between $\langle \kappa_p \rangle$ and $\langle \kappa_d \rangle$ as $\langle \kappa_p \rangle / \langle \kappa_d \rangle \simeq \exp(\alpha_{max})/\exp(-\alpha_{min}) = \exp(\alpha_{max} + \alpha_{min})$. Again, since $\alpha_{min} \ll \alpha_{max}$, I obtain

$$\frac{\langle \kappa_p \rangle}{\langle \kappa_d \rangle} \simeq \kappa_{p,max}. \tag{7}$$

This relation suggests that the ratio of the average adsorption rate constant to the average desorption rate constant is predominantly determined by the maximum adsorption rate constant, $\kappa_{p,max}$.

The dominance of the adsorption rate constant shown in Eq. (7) is a consequence of the asymmetry between the adsorption and desorption of organic matter onto and off mineral surfaces. The association of biopolymers with minerals is generally accompanied by the alteration of three-dimensional structures (i.e., conformational changes), formation of new ionic and covalent bonds, and variations in vibrational modes, resulting in irreversible adsorption[11,44,45]. For example, conformational changes can unfold/uncoil biopolymers and align them along mineral surfaces, suppressing their rotational dynamics and limiting their access to microbial enzymes[11,45]. These processes significantly increase the waiting time for biopolymers to be desorbed from mineral surfaces (i.e., $\tau_d\uparrow$ and $\kappa_d\downarrow$) and even lead biopolymers' adsorption to be irreversible (i.e., $\tau_d \to \infty$ and $\kappa_d \to 0$). In order words, due to the asymmetry between adsorption and desorption processes, the net amount of protected organic matter formed in unit time primarily depends on adsorption rates. However, how are adsorption rates related to the variation of O_2 levels? I explore this next.

Stability and instability of Earth's oxygen cycle. As discussed above, I identify the physically protected component y_2 as buried organic matter, which is responsible for the accumulation of O_2 in Earth's atmosphere. In the ancient environments, the atmospheric pO_2 was low[1,2] and τ_{O_2} was short[10,27]. By definition, oxygen-exposure time τ_{O_2} is the length of time t that organic matter stays and decays in the presence of O_2; in other words, $\tau_{O_2} = t$ in oxic environments. When O_2 levels are sufficiently low (i.e., $\tau_{O_2} \to 0$), I have $y_1 = (1-f)y_0$ and $y_2 = fy_0$; in this case, Eq. (2) implies that $[d\langle y_2 \rangle/d\tau_{O_2}]_{\tau_{O_2}\to 0} = [\langle \kappa_p \rangle(1-f) - \langle \kappa_d \rangle f]y_0$. To investigate how $\langle y_2 \rangle$ changes with τ_{O_2} under such O_2-limiting conditions, I set $[d\langle y_2 \rangle/d\tau_{O_2}]_{\tau_{O_2}\to 0} = 0$ and obtain a critical condition: $\langle \kappa_p \rangle / \langle \kappa_d \rangle = f/(1-f)$. This equality indicates that, in O_2-deficient environments, if $\langle \kappa_p \rangle / \langle \kappa_d \rangle < f/(1-f)$, then $\langle y_2 \rangle$ decreases as τ_{O_2} increases; if $\langle \kappa_p \rangle / \langle \kappa_d \rangle > f/(1-f)$, then $\langle y_2 \rangle$ rises with an increase in τ_{O_2}. I substitute Eq. (7) into the critical condition and rewrite the latter as $\kappa_{p,max} = f/(1-f)$. Henceforth, I denote the ratio $f/(1-f)$ by $\kappa_p^\star$, which represents a critical value for $\kappa_{p,max}$.
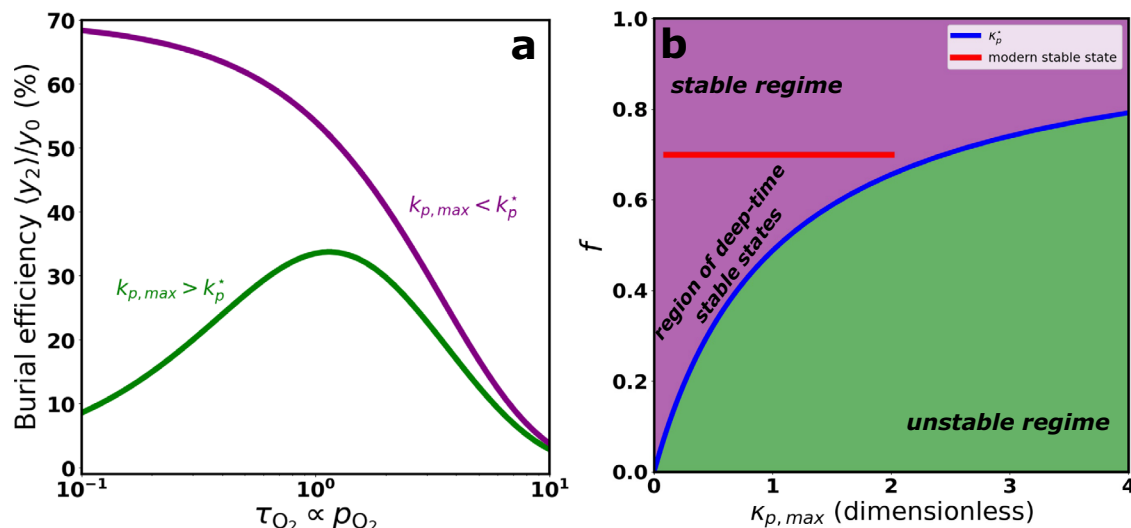
Fig. 2 Stability and instability of Earth's oxygen cycle in the parameter space of $(\kappa_{p,max}, f)$. a Burial efficiency $(\langle y_2 \rangle / y_0)$ versus oxygen exposure time $(\tau_{O_2} \propto pO_2)$ when $\kappa_{p,max} < \kappa_p^\star$ and $\kappa_{p,max} > \kappa_p^\star$. If $\kappa_{p,max} < \kappa_p^\star$ (purple curve), burial efficiency is high at low pO_2 and monotonically decreases as pO_2 increases. In this case, Earth's oxygen cycle is stabilized by a negative feedback loop. If $\kappa_{p,max} > \kappa_p^\star$ (green curve), burial efficiency first increases with pO_2 in the regime of low pO_2 and then declines as pO_2 further increases after passing a tipping point. In this case, negative feedback is absent at low pO_2, permitting the rise of O_2. Estimations based on the compiled datasets in Fig. 3 suggest that $\kappa_{p,max} \in (0.05, 2)$ and $f \simeq 0.7$ in the modern O_2-rich environment (refer to the following sections). The purple curve is generated with $\kappa_{p,max} = 0.5$ and $f = 0.7$ (i.e., $\kappa_p^\star \simeq 2$). Under the deep-time O_2-limiting conditions, $\kappa_{p,max}$ is expected to have been larger than its modern value while f is expected to have been smaller than its modern value (refer to the following sections). The green curve is generated with $\kappa_{p,max} = 3$ and $f = 0.1$ (i.e., $\kappa_p^\star \simeq 0.1$). **b** Parameter space of $(\kappa_{p,max}, f)$ for stable and unstable regimes of Earth's oxygen cycle. The borderline (blue) for the stable (purple) and unstable (green) regions is determined by $\kappa_p^\star = f/(1-f)$. The horizontal red line represents parameter values estimated from field observations in modern environments (i.e., $\kappa_{p,max} \in (0.05, 2)$ and $f \simeq 0.7$). The domain under the horizontal red line and left of the blue curve represents the region of $(\kappa_{p,max}, f)$ for the stable states in deep time (refer to the following sections). When mineral evolution causes a shift of Earth's oxygen cycle from the stable to the unstable region, Earth's oxygen cycle loses its stability, facilitating the accumulation of O_2.

Figure 2 illustrates how the burial efficiency of organic matter (i.e., $\langle y_2 \rangle / y_0$) changes with τ_{O_2} and therefore pO_2 in the two regimes divided by $\kappa_p^\star$ (blue curve in Fig. 2b). When $\kappa_{p,max} < \kappa_p^\star$ (purple curve in Fig. 2a and purple region in Fig. 2b), burial efficiency monotonically decreases with pO_2. However, when $\kappa_{p,max} > \kappa_p^\star$ (green curve in Fig. 2a and green region in Fig. 2b), burial efficiency increases with pO_2 in the region of low pO_2 and then declines as pO_2 further increases after passing a tipping point. In other words, whether burial efficiency and therefore the net O_2 production increase or decrease with pO_2 in the regime of low pO_2 depends on how much organic matter has been protected by minerals when it is initially deposited in sediments (i.e., f) and how large adsorption rates can be (i.e., $\kappa_{p,max}$).

When the initial fraction of protected organic matter is sufficiently high (i.e., a large f value), the capacity of mineral surfaces for further adsorption would be limited. Studies have shown that a larger initial coverage of organic matter on mineral surfaces would lead to higher repulsive barriers and therefore slower adsorption rates (i.e., a small $\kappa_{p,max}$ value)[25,46,47]. In this case (i.e., a large f and a small $\kappa_{p,max}$), O_2 starts to inhibit the burial of organic matter when it is deposited in sediments; the amount of buried organic matter and therefore the net production of O_2 monotonically decline as pO_2 increases (purple curve in Fig. 2a and purple region in Fig. 2b). This relation is analogous to the negative feedback stabilizing the modern atmospheric O_2 levels[11,27]. However, when the fraction of protected organic matter at the initial time point is low, mineral surfaces would have large capacities for further adsorption; in the meantime, the adsorption rates would be high due to the low repulsive barriers. Under such a condition (i.e., a small f and a large $\kappa_{p,max}$), unprotected organic matter continues to be

adsorbed onto mineral surfaces and O_2 does not immediately limit the burial of organic matter when it deposits in sediments. In this case, there exists an unstable regime in which negative feedback is absent, permitting O_2 to continuously accumulate (green curve in Fig. 2a and green region in Fig. 2b). When the maximum adsorption capacity is reached, no more organic matter can be adsorbed onto mineral surfaces; negative feedback again starts to operate, and the amount of buried organic matter declines with a further increase in O_2 (green curve in Fig. 2a).

Did mineral evolution facilitate Earth's oxidation? – Investigation via Fermi estimation. The theoretical analyses above explore the influence of organic matter-mineral interactions on the stability/instability of Earth's oxygen cycle; whether and how mineral evolution might have contributed to oxygenation events require investigation under the ancient circumstances. The values of parameters characterizing organic matter-mineral interactions in paleoenvironments, however, are currently unavailable. Here, I employ Fermi estimation[48,49] to explore the influence of mineral evolution on the oxygen cycle in deep time with modern parameter values as benchmarks[50]. Fermi estimation refers to the technique of studying complex problems, the exact solutions to which require extensive theoretical analysis or experimental investigation, via systematically dividing them into multiple parts and solving them with basic arithmetic[48,49]. To do so, I break down the problem—the influence of mineral evolution on Earth's oxidation—into three subproblems and investigate each one in the following sections. First, I estimate $\kappa_{p,max}$ and $\kappa_p^\star$ in the modern environment, denoted as $\kappa_{(p,max),Modern}$ and $\kappa_{p,Modern}^\star$, using data compiled from field observations. Second, I suggest that $\kappa_{(p,max),Modern}$ and $\kappa_{p,Modern}^\star$ can be used as references to test

whether mineral evolution destabilized the oxygen cycle and facilitated O_2 accumulation in deep time. Finally, with $\kappa_{(p,max),Modern}$ and $\kappa^\star_{p,Modern}$ as benchmarks, I propose that the evolution of iron and clay minerals might have contributed to the rise in O_2 levels during the Archean-Proterozoic and Proterozoic-Phanerozoic transitions, respectively.

Parameters $\kappa^\star_p$ and $\kappa_{p,max}$ in the modern environment. To estimate the modern values of $\kappa_{p,max}$ and $\kappa^\star_p$, I first compile the data on burial efficiency versus oxygen exposure time (i.e., y_2/y_0 versus t_{O_2}) from field observations[27,51–54]. These data are presented in Fig. 3, which shows that burial efficiency declines logarithmically with oxygen exposure time; such a pattern has been shown to appear in the degradation of mineral-associated organic matter in sediments[11,55]. The value of burial efficiency (y_2/y_0) at the left time boundary (i.e., 10^{-3} year) in Fig. 3 is set as the initial burial efficiency ($y_2(0)/y_0 = f$). I apply least-square regression to analyze the compiled dataset (Fig. 3) and obtain $f \simeq 0.7$ on average, which implies $\kappa^\star_p = f/(1-f) \simeq 2$ in the modern environment.

The longest timescale of the observations presented in Fig. 3 is 10^3 years; geological research, however, has suggested that organic matter can persist for millions of years in sediments[11,56]. Therefore, the timescale for organic matter degradation should range from 10^{-3} to 10^6 years. Since the unprotected component y_1 rapidly decays to CO_2, I take the rate constant corresponding to the shortest timescale as the characteristic degradation rate constant of the unprotected component, i.e., $k_1 \simeq 1/(10^{-3}$ year$)$. The degradation of the protected component y_2 is slower and depends on its interactions with minerals; I assume that its characteristic degradation rate constant k_2 falls between $1/(10^6$ year$)$ and k_1. Thus, $1/(10^6$ year$) \lesssim k_2 < k_1 \simeq 1/(10^{-3}$ year$)$. Again, I convert k_1 and k_2 to dimensionless quantities and obtain $\kappa_1 = 1$ and $\kappa_2 \in (10^{-9}, 1)$. As previously discussed, $\kappa_d \simeq \kappa_2$; therefore, substituting $\kappa_{2,min} = 10^{-9}$ and $\kappa_{2,max} = 1$ into Eq. (6) gives the average desorption rate constant: $\langle \kappa_d \rangle \simeq \langle \kappa_2 \rangle \simeq 0.05$. On the other hand, $\langle \kappa_d \rangle$ should be no greater than $\langle \kappa_p \rangle$; otherwise, all of the protected component y_2 would eventually decay to CO_2 and no protected organic matter would exist in the modern environment. This implies that $0.05 \simeq \langle \kappa_d \rangle \leq \langle \kappa_p \rangle < \kappa_{p,max}$. The modern Earth's oxygen cycle is maintained at a stable state by some negative feedback mechanisms[1,27], implying that $\kappa_{p,max}$ should be less than $\kappa^\star_p = 2$ (Fig. 2). Therefore, $\kappa_{p,max}$ should fall between 0.05 and 2 in the modern environment.

The red horizontal line in Fig. 2b represents the estimated parameter ranges under Earth's modern conditions: $0.05 < \kappa_{(p,max),Modern} < 2$ and $f_{Modern} \simeq 0.7$. The ranges of $\kappa_{p,max}$ and f in deep time, nevertheless, remain unknown, preventing the direct determination of their exact positions in the parameter space (Fig. 2b). In the next section, I suggest that $\kappa_{(p,max),Modern}$ and f_{Modern} can be used as references for deep time, providing an alternative approach to test whether mineral evolution contributed to oxygenation events on the ancient Earth.

Modern $\kappa_{p,max}$ and $\kappa^\star_p$ as benchmarks for deep time. The diversity of minerals on Earth's surface increased over geologic time as new mineral-generating processes, such as crust-mantle reworking and biological activities, came into play[3,4]. The abundance of terrestrial and riverine minerals, including those contributing to the physical protection of organic matter (e.g., iron(III) and clay minerals[11,57,58]), in deep time should have been lower than that in the modern environment[3,59]. Geological and biological evolution altered the residence times of organic matter on land as well. The growth of the land fraction on Earth's surface during the Archean-Proterozoic transition[60,61] might have remarkably elevated the length of time that organic matter stayed on the continents. Moreover, the Phanerozoic evolution of plant life significantly enhanced riverbank cohesion and reduced migration rates of meandering rivers[62,63], leading to longer residence times of organic matter in floodplains[64,65]. The lower abundances of terrestrial and riverine minerals and shorter residence times of organic matter on land in the Archean and Proterozoic likely resulted in less pre-formed association of organic matter with minerals (before being deposited in marine sediments) than in the modern, implying that $f_{Archean}$ and $f_{Proterozoic}$ are less than $f_{Modern} \simeq 0.7$ and therefore $\kappa^\star_{p,Archean}$ and $\kappa^\star_{p,Proterozoic}$ are less than $\kappa^\star_{p,Modern} \simeq 2$. On the other hand, a larger initial coverage of organic matter on mineral surfaces would lead to higher repulsive barriers and thus slower adsorption kinetics[25,46,47]; the relation between $\kappa_{p,max}$ and f is expressed as $\kappa_{p,max} \propto \exp(-f)$[25,26], which implies that $\kappa_{(p,max),Archean}$ and $\kappa_{(p,max),Proterozoic}$ are larger than $\kappa_{(p,max),Modern} > 0.05$. These estimations suggest that the deep-time stable regime in the parameter space is the domain under the horizontal red line and left of the blue curve in Fig. 2b.

I denote the ratio of $\kappa^\star_p$ to $\kappa_{p,max}$ by $R = \kappa^\star_p/\kappa_{p,max}$, which measures the change in $\kappa_{p,max}$ required to cross the boundary curve $\kappa^\star_p$ and switch from the stable to the unstable regime (Fig. 2b). The analyses above suggest that $R_{Archean}$ and $R_{Proterozoic}$ are less than R_{Modern}, which means that a larger increase in $\kappa_{p,max}$ is required to destabilize Earth's oxygen cycle in the modern (the horizontal red line in Fig. 2b) than in the Archean and Proterozoic (i.e., the region under the horizontal red line and left of the blue curve in Fig. 2b). In other words, if a growth in $\kappa_{p,max}$ is able to instigate Earth's oxygenation under the modern conditions, then so, too, it should have been in the Archean and Proterozoic environments. The relation $0.05 < \kappa_{(p,max),Modern} < \kappa^\star_{p,Modern} \simeq 2$ implies $R_{Modern} \leq 40$, which suggests that, if the Archean or Proterozoic mineral evolution resulted in a 40-fold or higher increase in $\kappa_{(p,max)}$, then Earth's oxygen cycle would have shifted into an unstable regime, facilitating the rise of O_2. In the following, I use $\kappa_{(p,max),Modern}$ and $\kappa^\star_{p,Modern}$ as benchmarks to investigate whether and how the evolution of iron and clay minerals contributed to the GOE and NOE, respectively.
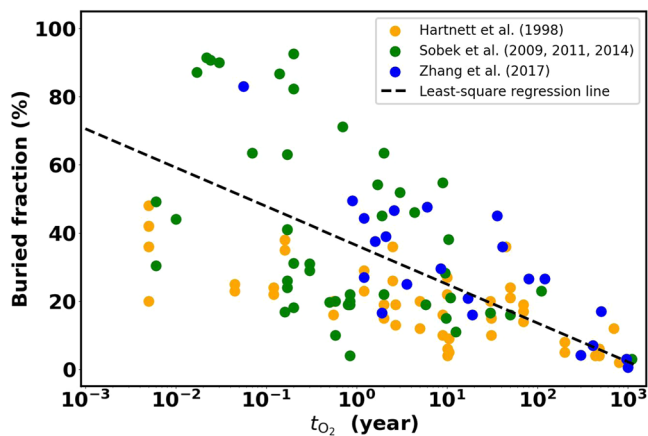

Fig. 3 The relation between the buried fraction of organic matter and oxygen exposure time in modern sediments. Data are compiled from the studies by Hartnett et al.[27] (yellow circles), Sobek et al.[51–53] (green circles), and Zhang et al.[54] (blue circles). The mathematical expression of the least-square regression (black dashed line) for the data is "buried fraction = $-9.90 \times \log_{10}(t_{O_2}) + 38.43$". The buried fraction at the left boundary, $t_{O_2} = 10^{-3}$ year, is around 70%.
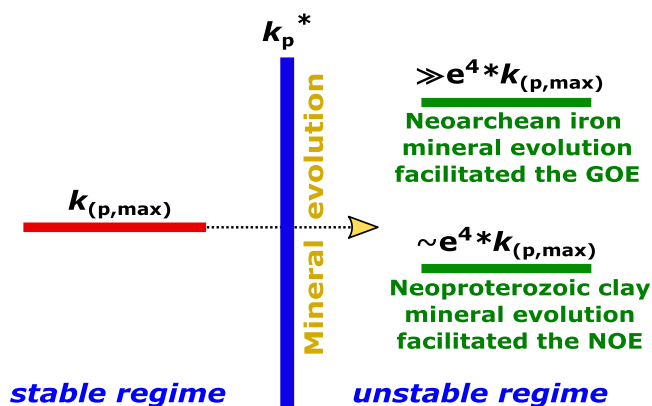
Fig. 4 Influence of iron and clay mineral evolution on Earth's oxygen cycle in deep time. Theoretical analyses in this study suggest that the Neoarchean transformation of dissolved iron(II) to ferrihydrite/iron(III) oxides and the Neoproterozoic production of weathering-derived clay minerals likely induced a $\gg e^4$-fold and $\sim e^4$-fold growth in $\kappa_{(p,max)}$, respectively. These increases are greater than the estimated 40-fold rise in $\kappa_{(p,max)}$ required to cross the critical value κ_p^* (Fig. 2b), suggesting that the Neoarchean evolution of iron minerals and Neoproterozoic evolution of clay minerals might have destabilized Earth's oxygen cycle and facilitated O_2 accumulation.

Iron mineral evolution and the GOE. Iron(III) minerals play a significant role in preserving organic matter in the modern environment[11,57,66]. Amorphous ferrihydrite and crystalline iron(III) oxides promote the persistence of organic matter in natural ecosystems via different mechanisms such as co-precipitation, direct chelation, and inner-sphere interactions[57,66]. However, its reduced state, iron(II), which is commonly soluble in natural aquatic systems, has a much weaker affinity to organic matter[67,68]; as a result, the contribution of iron(II) to the protection of organic matter is generally negligible[69,70]. In the Neoarchean O_2-deficient world, the majority of iron existed in the form of dissolved iron(II)[8,71]; the availability of iron(III) minerals was limited[8,71]. In such an environment, the transformation of dissolved iron(II) to iron(III) minerals, either through the direct iron-oxidation in photoferrotrophy[72,73] or via the reaction with O_2 produced by oxygenic photosynthesis[72,74], probably promoted the protection of organic matter, elevating O_2 levels on Earth's surface. Here, I explore this possibility by investigating the variations in the parameter space presented in Fig. 2b.

To justify whether the Neoarchean evolution of iron minerals contributed to the GOE, I first consider the molar ratios of the protected organic matter to iron(II) and to iron(III), which are henceforth denoted as OM:Fe(II) and OM:Fe(III), respectively. As mentioned above, the association of organic matter with iron(II) is basically negligible[66,68], implying that OM:Fe(II) $\ll 1$. On the other hand, global-scale observations in modern marine sediments have suggested that organic matter is associated with iron(III) (via co-precipitation/chelation) with OM:Fe(III) ≥ 4[57,67,75]. Therefore, the Neoarchean transformation of iron(II) to iron(III) likely resulted in a $\gg 4$ times increase in the capacity for organic matter-mineral associations. Since $\kappa_{p,max}$ is an e-folding function of capacity[25,26], a $\gg 4$-fold growth in capacity implies a $\gg e^4$ times rise in $\kappa_{p,max}$. A $\gg e^4$-fold change appears very large; experimental research, however, has shown that the rate constants of organic matter-mineral associations can vary across several orders of magnitude[76]. With $\kappa_{(p,max),Modern}$ and $\kappa_{p,\,Modern}^*$ as benchmarks, this $\gg e^4$-fold growth in $\kappa_{p,max}$ suggests that the Neoarchean evolution of iron minerals might have contributed to the GOE because such an increase is greater than

the estimated threshold of 40-fold growth required to destabilize the oxygen cycle and facilitate the rise of O_2 (Fig. 4).

The most prominent geological observation that appears to depart from the theory here is the scarcity of organic matter in iron formations, which were widely deposited during the Neoarchean and contain iron(III) oxides such as magnetite and hematite[72,77]. The deficiency of organic matter in iron formations has been attributed to its desorption during the aging of reactive ferrihydrite in diagenetic processes[78,79]. However, a large fraction ($\sim 23-27\%$) of the total organic matter remains bound to iron(III) in mature sediments on the modern Earth[57], and the fate of desorbed organic matter in the Neoarchean environment remains poorly understood. Although a substantial portion of the organic matter released during the diagenesis might have been remineralized with O_2 as the final electron acceptor[80,81], the rest was probably consumed in the temperature/pressure diagenesis (in the absence of O_2)[82] or sequestered/immobilized in deep sediments[13,22]. Moreover, experimental studies have suggested that ferrihydrite aging may instead enhance the stabilization of organic matter under certain natural conditions[83–85], which adds another layer of complexity to predicting the fate of organic matter associated with reactive iron(III) phases. Future field and laboratory investigations of organic matter bound to ferrihydrite/iron(III) oxides in diagenetic processes under conditions analogous to the Archean environment would offer validation of these speculations.

Clay mineral evolution and the NOE. Clays are the other major type of minerals contributing to the long-term preservation of organic matter on the modern Earth[11,58]. However, not all types of clay minerals were created equal in terms of their surface areas and therefore adsorption capacities over geologic time; whether and how clay mineral evolution contributed to the NOE remain debated[7,59,86]. The "clay mineral factory" hypothesis[7] proposed that the enhanced production of pedogenic phyllosilicates (e.g., smectites and kaolinites), which are weathering-derived and have high absorption capacity[47,58], during the Neoproterozoic might have promoted the burial of organic matter and therefore the accumulation of O_2. Nevertheless, other studies suggested that pedogenic phyllosilicates had developed well prior to the Proterozoic-Phanerozoic boundary[59] and the clay minerals formed during the Neoproterozoic were likely dominated by micas and tectosilicates/feldspars[86], which are inherited largely from parent rocks and possess low absorption capacities[47,58]. Here, instead of investigating the predominance of inherited versus pedogenic clays on the Neoproterozoic Earth's surface, I explore whether and how clay mineral evolution might have led to a shift from the stable to the unstable regime in the parameter space (Fig. 2b).

Earth's geosphere and biosphere underwent significant evolution in the Phanerozoic; the Neoproterozoic production of clay minerals therefore was likely to have differed significantly from that in the modern[3,59]. The intensity of oxidative weathering, which remarkably influences clay formation[59,87] and is positively correlated with the atmospheric O_2 level[13,88], should have been lower during the Neoproterozoic than in the present. The production flux of terrigenous minerals deriving from oxidative weathering, F_{ow}, is generally expressed as a function of atmospheric O_2 levels[88,89]: $F_{ow} \propto (pO_2)^{1/2}$. The pO_2, as suggested by geological and geochemical studies[74,90,91], increased by about $10-100$ times during the Late Neoproterozoic, implying a 3- to 10-fold rise in the production flux of weathering-derived clays and therefore in the surface capacity for organic matter association. This range is basically consistent with the estimated 4-fold growth in the surface capacity caused by the enhanced production of pedogenic phyllosilicate during the Neoproterozoic-Cambrian transition[7]. Here, I take this 4-fold rise[7]

for the analysis. As discussed in the last section, such a 4 times increase in adsorption capacity corresponds to an e^4-fold rise in $\kappa_{p,max}$. Again, with $\kappa_{(p,max),Modern}$ and $\kappa^{\star}_{p,Modern}$ as benchmarks, this growth induced by the evolution of clay minerals is higher than the estimated threshold of 40-fold elevation required to destabilize the oxygen cycle and promote the rise of O_2 (Fig. 4).

The theoretical analysis so far has explored the possible role of clay minerals in the NOE; the specific sources of weathering-derived clays in the Neoproterozoic are not well known. In addition to the inherited and pedogenic clays discussed in previous studies[7,86], other possible sources of clays remain understudied. The highly weatherable mafic and ultramafic rocks in large igneous provinces[92,93] and ophiolites[94,95] may serve as the sources of a variety of clay minerals with high absorption capacity, especially the smectite group. The emplacement and weathering of continental flood basalts and ophiolites in the Neoproterozoic[96,97] might have produced substantial clay minerals possessing large surface areas and enhanced the burial of organic matter. Moreover, the Neoproterozoic distribution, abundance, and evolution of authigenic iron(III)-bearing clays such as vermiculite, nontronite, chamosite, and glauconite deserve more investigation. The increased availability of ferric iron[3] and elevated intensity of reverse weathering[98] during the Neoproterozoic probably promoted the production of authigenic iron(III)-bearing clays[59,99], facilitating organic matter preservation and therefore O_2 accumulation.

Implications and limitations. The results presented here suggest several approaches for further exploring the role that minerals played in Earth's oxidation. In addition to ferrihydrite/iron(III) oxides and clays, other types of minerals such as calcites and biogenic opals[11,20] probably contributed to the accumulation of O_2 in deep time as well. Future studies on the evolutionary history of these minerals and their absorptive abilities in the paleoenvironment would support or falsify this speculation. Furthermore, this study uses parameter values estimated from observations in the modern environment (Fig. 3) as references to explore deep-time variations. Laboratory investigations of organic matter-mineral interactions under conditions analogous to Earth's ancient, especially the Neoarchean and Neoproterozoic, environments may offer precise parameter values and provide validation for the theory presented here. Besides, geochemical studies of the changes of mineral-associated organic matter abundance in sedimentary records over geologic time, especially during the periods of Earth's oxygenation events, possibly using ramped pyrolysis/oxidation[21,100], would offer direct support for the mechanisms proposed in this work.

The physical interactions and chemical reactions in the system of organic matter, minerals, and O_2 are interwoven and complex; the theoretical results obtained from the mathematical model (Eqs. (1) and (2)), such as the probability distribution of adsorption/desorption rate constants (Eq. (5)) and the stable/unstable regimes of Earth's oxygen cycle (Fig. 2), are based on simplified and idealized assumptions. The 40-fold growth of $\kappa_{p,max}$ required to destabilize the oxygen cycle (Fig. 4) is therefore a rough estimation; high-dimensional models with more general assumptions may offer more realistic predictions. Moreover, this study investigates how mineral evolution might have influenced O_2 levels via affecting organic matter-mineral interactions (Fig. 1); variables directly characterizing the evolution of minerals are not explicitly included in the minimalistic model (Eqs. (1) and (2)). Parameterizing these variables in the present theoretical framework would provide deeper insights into the contribution of mineral evolution to Earth's oxygenation. In addition, the geochemically-based model in this study does not consider biological processes, which can

significantly influence the production/consumption of organic matter and O_2 and the physical/chemical proterites of minerals[11,24]. Integrating biological factors into the model presented here may provide a more comprehensive understanding of how the changes in biosphere might have influenced O_2 levels on Earth's surface via inducing mineral evolution.

In summary, this work explores whether and how organic matter-mineral interactions might have contributed to Earth's oxidation in deep time. Although the theoretical results and proposed mechanisms require further experimental and field justification, this study links for the first time the microscopic interactions between organic matter and minerals to the macroscopic dynamics (i.e., stability/instability) of Earth's oxygen cycle. These results may provide a step toward a quantitative understanding of how mineral evolution has shaped the surface environments of Earth and exoplanets.

Data availability
Data sharing not applicable to this article as no datasets were generated during the current study.

References
1. Canfield, D. E. *Oxygen: A Four Billion Year History* (Princeton University Press, 2014).
2. Lyons, T. W., Reinhard, C. T. & Planavsky, N. J. The rise of oxygen in Earth's early ocean and atmosphere. *Nature* **506**, 307–315 (2014).
3. Hazen, R. M. et al. Mineral evolution. *Am. Mineral.* **93**, 1693–1720 (2008).
4. Hazen, R. M. & Ferry, J. M. Mineral evolution: mineralogy in the fourth dimension. *Elements* **6**, 9–12 (2010).
5. Pufahl, P. K. & Hiatt, E. E. Oxygenation of the Earth's atmosphere-ocean system: a review of physical and chemical sedimentologic responses. *Mar. Pet. Geol.* **32**, 1–20 (2012).
6. Hummer, D. R. et al. Evidence for the oxidation of Earth's crust from the evolution of manganese minerals. *Nat. Commun.* **13**, 960 (2022).
7. Kennedy, M., Droser, M., Mayer, L. M., Pevear, D. & Mrofka, D. Late Precambrian oxygenation; inception of the clay mineral factory. *Science* **311**, 1446–1449 (2006).
8. Holland, H. D. The oxygenation of the atmosphere and oceans. *Philos. Trans. R. Soc. B: Biol. Sci.* **361**, 903–915 (2006).
9. Shang, H., Rothman, D. H. & Fournier, G. P. Oxidative metabolisms catalyzed Earth's oxygenation. *Nat. Commun.* **13**, 1–9 (2022).
10. Hedges, J. I. & Keil, R. G. Sedimentary organic matter preservation: an assessment and speculative synthesis. *Mar. Chemistry* **49**, 81–115 (1995).
11. Keil, R. G. & Mayer, L. M. Mineral matrices and organic matter. In *Treatise on Geochemistry*, Vol. 12 (eds. Holland, H. D. & Turekian, K. K.) 337–359 (Elsevier, Oxford, 2014).
12. Sparkes, R. B., Hovius, N., Galy, A. & Liu, J. T. Survival of graphitized petrogenic organic carbon through multiple erosional cycles. *Earth Planet. Sci. Lett.* **531**, 115992 (2020).
13. Galvez, M. E., Fischer, W. W., Jaccard, S. L. & Eglinton, T. I. Materials and pathways of the organic carbon cycle through time. *Nat. Geosci.* **13**, 535–546 (2020).
14. Wershaw, R. Model for humus in soils and sediments. *Environ. Sci. Technol.* **27**, 814–816 (1993).
15. Rashid, M. A. *Geochemistry of Marine Humic Compounds* (Springer Science & Business Media, 2012).
16. Galy, V., Beyssac, O., France-Lanord, C. & Eglinton, T. Recycling of graphite during Himalayan erosion: a geological stabilization of carbon in the crust. *Science* **322**, 943–945 (2008).
17. Jannasch, H. W. The microbial turnover of carbon in the deep-sea environment. *Glob. Planet. Change* **9**, 289–295 (1994).
18. Arrieta, J. M. et al. Dilution limits dissolved organic carbon utilization in the deep ocean. *Science* **348**, 331–333 (2015).
19. Vindedahl, A. M., Strehlau, J. H., Arnold, W. A. & Penn, R. L. Organic matter and iron oxide nanoparticles: aggregation, interactions, and reactivity. *Environ. Sci.: Nano* **3**, 494–505 (2016).
20. Kleber, M. et al. Dynamic interactions at the mineral-organic matter interface. *Nat. Rev. Earth Environ.* **2**, 402–421 (2021).

21. Hemingway, J. D. et al. Mineral protection regulates long-term global preservation of natural organic carbon. *Nature* **570**, 228–231 (2019).

22. Hayes, J. M. & Waldbauer, J. R. The carbon cycle and associated redox processes through time. *Philos. Trans. R. Soc. B: Biol. Sci.* **361**, 931–950 (2006).

23. Middelburg, J. J. A simple rate model for organic matter decomposition in marine sediments. *Geochimica et Cosmochimica Acta* **53**, 1577–1581 (1989).

24. Arndt, S. et al. Quantifying the degradation of organic matter in marine sediments: a review and synthesis. *Earth-Sci. Rev.* **123**, 53–86 (2013).

25. Gu, B., Schmitt, J., Chen, Z., Liang, L. & McCarthy, J. F. Adsorption and desorption of natural organic matter on iron oxide: mechanisms and models. *Environ. Sci. Technol.* **28**, 38–46 (1994).

26. Fava, A. & Eyring, H. Equilibrium and kinetics of detergent adsorption – a generalized equilibration theory. *J. Phys. Chem.* **60**, 890–898 (1956).

27. Hartnett, H. E., Keil, R. G., Hedges, J. I. & Devol, A. H. Influence of oxygen exposure time on organic carbon preservation in continental margin sediments. *Nature* **391**, 572–575 (1998).

28. Beulig, F., Røy, H., Glombitza, C. & Jørgensen, B. B. Control on rate and pathway of anaerobic organic carbon degradation in the seabed. *Proc. Natl Acad. Sci. USA* **115**, 367–372 (2018).

29. Bowles, M. W., Mogollón, J. M., Kasten, S., Zabel, M. & Hinrichs, K.-U. Global rates of marine sulfate reduction and implications for sub–sea-floor metabolic activities. *Science* **344**, 889–891 (2014).

30. Lane, N. & Martin, W. The energetics of genome complexity. *Nature* **467**, 929–934 (2010).

31. Douglas, J. F., Johnson, H. E. & Granick, S. A simple kinetic model of polymer adsorption and desorption. *Science* **262**, 2010–2012 (1993).

32. Douglas, J. F. Polymer localization by random fixed impurities: Gaussian chains. *Macromolecules* **21**, 3515–3519 (1988).

33. Frantz, P. & Granick, S. Kinetics of polymer adsorption and desorption. *Phys. Rev. Lett.* **66**, 899 (1991).

34. Frantz, P. & Granick, S. Exchange kinetics of adsorbed polymer and the achievement of conformational equilibrium. *Macromolecules* **27**, 2553–2558 (1994).

35. Shang, H. A generic hierarchical model of organic matter degradation and preservation in aquatic systems. *Commun. Earth Environ.* **4**, 16 (2023).

36. Montroll, E. W. & Shlesinger, M. F. On $1/f$ noise and other distributions with long tails. *Proc. Natl Acad. Sci. USA* **79**, 3380–3383 (1982).

37. Amir, A., Oreg, Y. & Imry, Y. On relaxations and aging of various glasses. *Proc. Natl Acad. Sci. USA* **109**, 1850–1855 (2012).

38. Phillips, J. Stretched exponential relaxation in molecular and electronic glasses. *Rep. Prog. Phys.* **59**, 1133 (1996).

39. Amir, A., Oreg, Y. & Imry, Y. Slow relaxations and aging in the electron glass. *Phys. Rev. Lett.* **103**, 126403 (2009).

40. Ansari, A. et al. Protein states and proteinquakes. *Proc. Natl Acad. Sci. USA* **82**, 5000–5004 (1985).

41. Dewey, T. G. & Bann, J. G. Protein dynamics and $1/f$ noise. *Biophys. J.* **63**, 594–598 (1992).

42. Ben-David, O., Rubinstein, S. M. & Fineberg, J. Slip-stick and the evolution of frictional strength. *Nature* **463**, 76–79 (2010).

43. Persson, B. N. Theory of friction: stress domains, relaxation, and creep. *Phys. Rev. B* **51**, 13568 (1995).

44. Van Tassel, P. R., Viot, P., Tarjus, G. & Talbot, J. Irreversible adsorption of macromolecules at a liquid-solid interface: theoretical studies of the effects of conformational change. *J. Chem. Phys.* **101**, 7064–7073 (1994).

45. Kim, J. M. & Baig, C. Precise analysis of polymer rotational dynamics. *Sci. Rep.* **6**, 1–7 (2016).

46. Peterson, C. & Kwei, T. The kinetics of polymer adsorption onto solid surfaces. *J. Phys. Chem.* **65**, 1330–1333 (1961).

47. Theng, B. K. *Formation and Properties of Clay-Polymer Complexes* (Elsevier, 2012).

48. Weinstein, L. & Adam, J. A. *Guesstimation* (Princeton University Press, 2009).

49. Von Baeyer, H. C. *The Fermi Solution: Essays on Science* (Courier Corporation, 2001).

50. Lyell, C. *Principles of Geology: Being an Attempt to Explain the Former Changes of the Earth's Surface, by Reference to Causes Now in Operation* (John Murray, 1830).

51. Sobek, S. et al. Organic carbon burial efficiency in lake sediments controlled by oxygen exposure time and sediment source. *Limnol. Oceanogr.* **54**, 2243–2254 (2009).

52. Sobek, S., Zurbrügg, R. & Ostrovsky, I. The burial efficiency of organic carbon in the sediments of Lake Kinneret. *Aquat. Sci.* **73**, 355–364 (2011).

53. Sobek, S., Anderson, N., Bernasconi, S. & Del Sontro, T. Low organic carbon burial efficiency in arctic lake sediments. *J. Geophys. Res.: Biogeosci.* **119**, 1231–1243 (2014).

54. Zhang, S. et al. The oxic degradation of sedimentary organic matter 1400 Ma constrains atmospheric oxygen levels. *Biogeosciences* **14**, 2133–2149 (2017).

55. Coppola, L. et al. The importance of ultrafine particles as a control on the distribution of organic carbon in Washington Margin and Cascadia Basin sediments. *Chem. Geol.* **243**, 142–156 (2007).

56. Dittmar, T. et al. Enigmatic persistence of dissolved organic matter in the ocean. *Nat. Rev. Earth Environ.* **2**, 570–583 (2021).

57. Lalonde, K., Mucci, A., Ouellet, A. & Gélinas, Y. Preservation of organic matter in sediments promoted by iron. *Nature* **483**, 198–200 (2012).

58. Blattmann, T. M. et al. Mineralogical control on the fate of continentally derived organic matter in the ocean. *Science* **366**, 742–745 (2019).

59. Hazen, R. M. et al. Clay mineral evolution. *Am. Mineral.* **98**, 2007–2029 (2013).

60. McLennan, S. M. & Taylor, S. Geochemical constraints on the growth of the continental crust. *J. Geol.* **90**, 347–361 (1982).

61. Krissansen-Totton, J., Arney, G. N. & Catling, D. C. Constraining the climate and ocean pH of the early Earth with a geological carbon cycle model. *Proc. Natl Acad. Sci. USA* **115**, 4105–4110 (2018).

62. Ielpi, A. & Lapôtre, M. G. A tenfold slowdown in river meander migration driven by plant life. *Nat. Geosci.* **13**, 82–86 (2020).

63. Ielpi, A., Lapôtre, M. G., Gibling, M. R. & Boyce, C. K. The impact of vegetation on meandering rivers. *Nat. Rev. Earth Environ.* **3**, 165–178 (2022).

64. Torres, M. A. et al. Model predictions of long-lived storage of organic carbon in river deposits. *Earth Surf. Dyn.* **5**, 711–730 (2017).

65. Douglas, M. M. et al. Organic carbon burial by river meandering partially offsets bank erosion carbon fluxes in a discontinuous permafrost floodplain. *Earth Surf. Dyn.* **10**, 421–435 (2022).

66. Barber, A. et al. Preservation of organic matter in marine sediments by inner-sphere interactions with reactive iron. *Sci. Rep.* **7**, 1–10 (2017).

67. Stumm, W. & Morgan, J. J. *Aquatic Chemistry: Chemical Equilibria and Rates in Natural Waters* (John Wiley & Sons, 2012).

68. Morel, F. M. & Hering, J. G. *Principles and Applications of Aquatic Chemistry* (John Wiley & Sons, 1993).

69. Nierop, K. G., Jansen, B. & Verstraten, J. M. Dissolved organic matter, aluminium and iron interactions: precipitation induced by metal/carbon ratio, pH and competition. *Sci. Total Environ.* **300**, 201–211 (2002).

70. Zhang, J., Dong, H., Zeng, Q. & Agrawal, A. The role of Fe(III) bioreduction by methanogens in the preservation of organic matter in smectite. *Chem. Geol.* **389**, 16–28 (2014).

71. Anbar, A. D. Elements and evolution. *Science* **322**, 1481–1483 (2008).

72. Konhauser, K. et al. Iron formations: a global record of Neoarchaean to Palaeoproterozoic environmental history. *Earth-Sci. Rev.* **172**, 140–177 (2017).

73. Crowe, S. A. et al. Photoferrotrophs thrive in an Archean Ocean analogue. *Proc. Natl Acad. Sci. USA* **105**, 15938–15943 (2008).

74. Canfield, D. E. The early history of atmospheric oxygen: homage to Robert M. Garrels. *Ann. Rev. Earth Planet. Sci.* **33**, 1–36 (2005).

75. Salvadó, J. A. et al. Organic carbon remobilized from thawing permafrost is resequestered by reactive iron on the Eurasian Arctic Shelf. *Geophys. Res. Lett.* **42**, 8122–8130 (2015).

76. Shaker, A. M., Komy, Z. R., Heggy, S. E. & El-Sayed, M. E. Kinetic study for adsorption humic acid on soil minerals. *J. Phys. Chem. A* **116**, 10889–10896 (2012).

77. Bekker, A. et al. Iron formation: the sedimentary product of a complex interplay among mantle, tectonic, oceanic, and biospheric processes. *Econ. Geol.* **105**, 467–508 (2010).

78. Jelavić, S., Mitchell, A. & Sand, K. Fate of organic compounds during transformation of ferrihydrite in iron formations. *Geochem. Perspect. Lett.* **15**, 25–29 (2020).

79. Faust, J. C. et al. Millennial scale persistence of organic carbon bound to iron in Arctic marine sediments. *Nat. Commun.* **12**, 275 (2021).

80. Walker, J. C. Suboxic diagenesis in banded iron formations. *Nature* **309**, 340–342 (1984).

81. Friese, A. et al. Organic matter mineralization in modern and ancient ferruginous sediments. *Nat. Commun.* **12**, 2216 (2021).

82. Posth, N. R. et al. Simulating Precambrian banded iron formation diagenesis. *Chem. Geol.* **362**, 66–73 (2013).

83. Lu, Y. et al. Ferrihydrite transformation under the impact of humic acid and Pb: kinetics, nanoscale mechanisms, and implications for C and Pb dynamics. *Environ. Sci.: Nano* **6**, 747–762 (2019).

84. Hu, S. et al. Kinetics of As(V) and carbon sequestration during Fe(II)-induced transformation of ferrihydrite-As(V)-fulvic acid coprecipitates. *Geochim. Cosmochim. Acta* **272**, 160–176 (2020).

85. Zhao, Y. et al. The role and fate of organic carbon during aging of ferrihydrite. *Geochim. Cosmochim. Acta* **335**, 339–355 (2022).

86. Tosca, N. J. et al. Clay mineralogy, organic carbon burial, and redox evolution in Proterozoic oceans. *Geochim. Cosmochim. Acta* **74**, 1579–1592 (2010).

87. Millot, G. *Geology of Clays: Weathering · Sedimentology · Geochemistry* (Springer Science & Business Media, 2013).

88. Lasaga, A. C. & Ohmoto, H. The oxygen geochemical cycle: dynamics and stability. *Geochim. Cosmochim. Acta* **66**, 361–381 (2002).

89. Lenton, T. M., Daines, S. J. & Mills, B. J. COPSE reloaded: an improved model of biogeochemical cycling over Phanerozoic time. *Earth-Sci. Rev.* **178**, 1–28 (2018).

90. Kump, L. R. The rise of atmospheric oxygen. *Nature* **451**, 277–278 (2008).

91. Reinhard, C. T. & Planavsky, N. J. The history of ocean oxygenation. *Ann. Rev. Mar. Sci.* **14**, 331–353 (2021).

92. Nesbitt, H. W. & Young, G. M. Prediction of some weathering trends of plutonic and volcanic rocks based on thermodynamic and kinetic considerations. *Geochim. Cosmochim. Acta* **48**, 1523–1534 (1984).

93. Coffin, M. F. & Eldholm O. Large igneous provinces: crustal structure, dimensions, and external consequences. *Rev. Geophys.* **32**, 1–36 (1994).

94. Dilek, Y. & Furnes, H. Ophiolites and their origins. *Elements* **10**, 93–100 (2014).

95. Macdonald, F. A., Swanson-Hysell, N. L., Park, Y., Lisiecki, L. & Jagoutz, O. Arc-continent collisions in the tropics set Earth's climate state. *Science* **364**, 181–184 (2019).

96. Cox, G. M. et al. Continental flood basalt weathering as a trigger for Neoproterozoic Snowball Earth. *Earth Planet. Sci. Lett.* **446**, 89–99 (2016).

97. Furnes, H., De Wit, M. & Dilek, Y. Four billion years of ophiolites reveal secular trends in oceanic crust formation. *Geosci. Front.* **5**, 571–603 (2014).

98. Li, F. et al. Reverse weathering may amplify post-Snowball atmospheric carbon dioxide levels. *Precambrian Res.* **364**, 106279 (2021).

99. Isson, T. T. & Planavsky, N. J. Reverse weathering as a long-term stabilizer of marine pH and planetary climate. *Nature* **560**, 471–475 (2018).

100. Hemingway, J. D. et al. Assessing the blank carbon contribution, isotope mass balance, and kinetic isotope fractionation of the ramped pyrolysis/oxidation instrument at NOSAMS. *Radiocarbon* **59**, 179–193 (2017).

Author contributions

H.S. conceived the project, performed the research, and wrote the manuscript.

Competing interests

The author declares no competing interests.

Additional information

Supplementary information The online version contains supplementary material available at https://doi.org/10.1038/s43247-023-00824-3.

Correspondence and requests for materials should be addressed to Haitao Shang.

Peer review information *Communications Earth & Environment* thanks Richard Boyle, Jordon Hemingway and the other, anonymous, reviewer(s) for their contribution to the peer review of this work. Primary Handling Editor: Joe Aslin. Peer reviewer reports are available.

Reprints and permission information is available at http://www.nature.com/reprints

Publisher's note Springer Nature remains neutral with regard to jurisdictional claims in published maps and institutional affiliations.